Makara Journal of Science

Volume 24
Issue 3 *September*

Article 6

9-18-2020

Key Deposition Parameters for Short-type ZnO Nanosheets Electrodeposited Under Galvanostatic Mode

Gerald Ensang Timuda
Research Center for Physics, Indonesian Institute of Sciences (P2F-LIPI), Building 442 Kawasan PUSPIPTEK, Banten 15314, Indonesia, gera001@lipi.go.id

Dhimas Harjanto
Department of Physics, Faculty of Science and Technology, Universitas Islam Negeri Syarif Hidayatullah Jakarta, Ciputat, 15412, Indonesia

Wahyu Bambang Widayatno
Research Center for Physics, Indonesian Institute of Sciences (P2F-LIPI), Building 442 Kawasan PUSPIPTEK, Banten 15314, Indonesia

Makara Journal of Science, 24/3 (2020), 179–187
doi: 10.7454/mss.v24i3.1202

Key Deposition Parameters for Short-type ZnO Nanosheets Electrodeposited Under Galvanostatic Mode

Gerald Ensang Timuda[1*], Dhimas Harjanto[2], and Wahyu Bambang Widayatno[1]

1. Research Center for Physics, Indonesian Institute of Sciences (P2F-LIPI), Building 442 Kawasan PUSPIPTEK, Banten 15314, Indonesia
2. Department of Physics, Faculty of Science and Technology, Universitas Islam Negeri Syarif Hidayatullah Jakarta, Ciputat, 15412, Indonesia

[*]*E-mail: gera001@lipi.go.id*

Received September 18, 2019 | Accepted April 2, 2020

Abstract

Studies on the deposition of ZnO nanosheets grown vertically and perpendicular to conductive substrates have been conducted to obtain tall-type nanosheets (approximately 15 µm in height). However, some applications require short-type nanosheets with a height of about 1µm or less. In this study, short-type ZnO nanosheets were electrodeposited on indium-doped tin oxide substrates under galvanostatic (constant current) mode for a short deposition time. Then, the key parameters to form nanosheet layers with a height in the micrometer order and with good coverage were evaluated. Deposition was performed at 1 mA/cm^2 for 60 s. Ar gas was initially bubbled into the electrolyte solution during electrodeposition to remove oxygen. Then, the solution was compared with solutions that did not undergo bubbling. Various electrolyte compositions (various concentrations of acetate and nitrate) were observed in solutions under the non-Ar bubbling condition. Moreover, the oxygen in the solution remarkably affected the morphology of the nanosheet, which became much denser and taller. Therefore, altering electrolyte composition affects morphology, although the effect is not as significant. Electrolyte composition must be optimized to produce the desired short and dense nanosheets because a low concentration of each anion leads to the production of a non-nanosheet layer, whereas a high concentration causes reduction in the density coverage of the nanosheet. A complete discussion of this phenomenon is presented in this study.

Keywords: electrolyte composition, galvanostatic electrodeposition, gas bubbling, short deposition time, zinc oxide nanosheet

Introduction

ZnO nanosheets are 2D materials that have attracted considerable attention because the material has been proposed as an interesting alternative to a more commonly used types of nanostructure such as nanoparticle or nanorod in several device applications. For example in dye-sensitized solar cells [1,2], ZnO nanosheets have been considered to be an alternative to widely used mesoporous or novel 1D structures, such as nanorods and nanowires. These nanosheets retain the beneficial features of the two structures (high surface area of mesoporous structures and high electron transport properties of 1D structures) to some extent and reduce their negative properties (low electron transport properties of the mesoporous structures and low surface area of 1D structures). Another example as piezoelectric material [3,4], these 2D nanosheets have higher ductility compared with its 1D counterpart; thus, it can receive higher pressure and can then produce a more robust piezoelectric.

In the examples mentioned above, typical tall-type nanosheets are required (approximately 10–20 µm in height). Thus, studies on the deposition of ZnO nanosheets have focused on tall and dense nanosheets. However, some applications require short-type nanosheets that can maintain good coverage over a substrate. For instance, in perovskite solar cells, the metal oxide layer used for the electron transport layer (ETL) must have a thickness of about 1 µm or less. Perovskite solar cells are a new type of solar cell that has undergone tremendous improvement in efficiency in less than a decade [5]. Naturally, these cells received wide attention from the research community as the most promising to achieve the goal of the 3rd-generation solar cells, which are cheap and efficient and contain nonprecious elements. The ETL is an important part of

the solar cell to extract the photoelectrons produced by the perovskite layer under illumination [6]. The electron and hole diffusion length in the mixed halide perovskite ($CH_3NH_3PbI_{3-x}Cl_x$) can be greater than 1 µm, whereas the triiodide counterpart ($CH_3NH_3PbI_3$) can be ~100 nm [7]. Therefore, the synthesis of nanostructured ETL in the order of 1 µm or less has become crucial; thus, its deposition method is interesting to be explored further.

To obtain this nanosheet structure, this study used the electrodeposition method. This method has several advantages over other methods, such as hydrothermal [8] and chemical bath deposition [9]; these advantages include strong attachment of the deposited film to the substrate, readiness for an upscale, relatively easy process, and good reproducibility. Previously, we have studied the electrodeposition of ZnO nanosheets under galvanostatic (constant current) mode and observed the limit of the deposition on the higher end of the properties by monitoring the effect of current and deposition time on the nanostructure [10]. By using galvanostatic electrodeposition for an adequate period, a unique double-layer structure, which comprises a nanosheet grown on top of a specific underlayer where the nanosheet forms a major part of the total height, was obtained[10]. Such characteristic is in contrast to that of structures formed under potentiostatic mode [2]. To obtain short-type nanosheets under galvanostatic mode in the order of a single micrometer height, short-time deposition (1 minute or less) could be used. However, even though a pure nanosheet structure could be obtained, the short nanosheet was grown scarcely, and it was not dense enough to be suitable for the perovskite solar cell's ETL layer. To the best of our knowledge, no study has discussed this specific type of short ZnO nanosheet; thus, its density/coverage issue has yet to be addressed. Therefore, the deposition method is further improved in this study by evaluating key deposition parameters.

To grow ZnO via electrodeposition, zinc and nitrate ions are essential in the electrolyte solution. During electrodeposition, the supplied electron is used to reduce nitrate and produce hydroxide (Eq. 1). Moreover, the oxygen contained in the electrolyte can produce hydroxide (Eq. 2) [11]. The hydroxides then react with the zinc ions to produce ZnO eventually (Eq. 3). In our previous study [10], the hydroxide formation route was only from nitrate reduction (Eq. 1) in which the oxygen contained in the electrolyte solution is removed using Ar bubbling. In the present study, the presence of oxygen is one of the parameters evaluated.

$$NO_3^- + H_2O + 2e^- \rightarrow NO_2^- + 2OH^- \quad (1)$$

$$O_2 + 2H_2O + 4e^- \rightarrow 4OH^- \quad (2)$$

$$Zn^{2+} + 2OH^- \rightarrow Zn(OH)_2 \rightarrow ZnO + H_2O \quad (3)$$

ZnO has a wurtzite hexagonal structure in atmospheric pressure and temperature and has a preferred growth orientation at (002) direction. The facet at this direction ends with Zn^{2+} atoms, making it a polar surface. By contrast, the facet at the direction perpendicular to it (e.g. (100)) ends with equal amounts of Zn^{2+} and O^{2-} atoms, making them a nonpolar surface. A certain nanostructure can be obtained by manipulating the crystal growth at a specific orientation. For example, promoting the growth at (002) can lead to the formation of a nanorod or nanowire, whereas suppressing it can lead to a nanosheet. Xu et al. [12] observed the formation of a hexagonal ZnO column vertically grown with a (002) orientation perpendicular to the ITO substrate via electrodeposition using $Zn(NO_3)_2$-based solution as the electrolyte. A column with a thinner diameter (i.e. nanowire) was obtained by adding hexamethylenetetramine in the electrolyte solution. The HTM addition resulted in the formation of $Zn(OH)_4^{2-}$, which then gathered at the polar (002) facet, promoting ZnO growth at this orientation and eventually producing a nanowire with a high aspect ratio. By contrast, a nanosheet structure was obtained when $Cl^-$was added. In this case, Cl^-similarly gathered at the polar (002) facet, thus hindering growth at this orientation and eventually promoting growth at directions perpendicular to it (e.g. (100) producing a nanosheet structure). In addition to Cl^-[12,13], other anions have been used as shaping agent to form nanosheets; these anions include SO_4^{2-}[14], acetate [2,15], Br^-[16], or high concentrations of nitrate[17]. However, the addition of the extra anions can cause the production of side products other than the ZnO shown in Eq. 3. In the present study, the anions contained in the electrolyte solution are acetate and nitrate. The side products that can be formed due to the presence of these two anions are $Zn_5(CH_3COO)_2(OH)_8 \cdot 2H_2O$ (Eq. 4) [15] and $Zn_5(OH)_8(NO_3)_2 \cdot 2H_2O$ (Eq. 5) [17], respectively.

$$5Zn^{2+} + 2CH_3COO^- + 8OH^- + 2H_2O \rightarrow Zn_5(CH_3COO)_2(OH)_8 \cdot 2H_2O \quad (4)$$

$$5Zn^{2+} + 2NO_3^- + 8OH^- + 2H_2O \rightarrow Zn_5(OH)_8(NO_3)_2 \cdot 2H_2O \quad (5)$$

Our previous study [10] has shown that for short deposition times (1 minute or less), the nanosheet formed contains two side products apart from ZnO. This result indicates that the presence of these two anions is important in the nanosheet formation at the initial deposition state; thus, their variation of concentration must be studied to improve the coverage of short-type nanosheets. Based on the above considerations, this study improves nanosheet deposition by evaluating the effect of the introduction of oxygen (from the air), coupled with the variation in acetate and nitrate concentrations. To the best of our knowledge, this study is the first to evaluate the effect of these deposition

parameters for short-type ZnO nanosheet structures. The effect of the key parameters on short-type ZnO nanosheets suitable as an ETL for perovskite solar cells is discussed in detail.

Methods

Materials were used as received. ZnO electrodeposition was performed under galvanostatic mode, with a two-electrode electrochemical system using indium-doped tin oxide (ITO) (7 Ω/□, MTI-USA) as the working electrode and zinc wire (99.995%, XL Alloy) as the counter electrode (Figure 1). The electrolyte was made from an aqueous solution of $Zn(NO_3)_2.4H_2O$ (Merck) and CH_3COOK (Himedia) with various concentrations. The default concentration was 0.05 M $Zn(NO_3)_2$ + 0.05 M CH_3COOK. To observe the effect of $Zn(NO_3)_2.4H_2O$ concentrations, the solution was varied from 0.03, 0.05, and 0.07 M while maintaining the CH_3COOK concentration at 0.05 M. Similarly, to observe the effect of CH_3COOK concentrations, it was varied from 0.01, 0.03, 0.05 and 0.07 M while maintaining the $Zn(NO_3)_2.4H_2O$ concentration at 0.05 M. The pH of the solution was controlled at approximately 6 by adding 0.1 M CH_3COOH to the solution dropwise. Electrodeposition was performed under galvanostatic mode using an applied current of 1 mA/cm^2 for 1 h and 60 s. For 1 h deposition, Ar gas was bubbled inside the electrolyte (20 ml/min.) for 30 minutes before and during electrodeposition to prevent the oxygen from the environment from mixing in the electrolyte. The same procedure was implemented for the 60 s deposition; then, the solution was compared with those without Ar introduction (open condition) to allow oxygen to remain in the electrolyte solution. The open condition was then maintained for the varied concentration experiments. The temperature during electrodeposition was kept at 60°C. After electrodeposition, the coated ITO sample was rinsed in distilled water and dried naturally. This as-deposited sample was then annealed at 400°C for 1 h to transform it into ZnO completely.

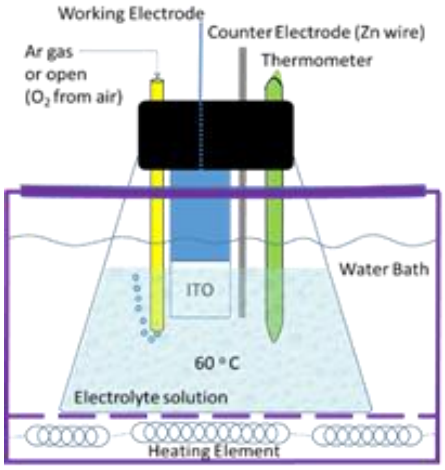

Figure 1. Schematic of the Experimental Setup

The as-deposited and annealed samples were then characterized via XRD (Rigaku Smartlab), SEM (Keyence VE-7800), and FE-SEM (Multibeam Focused Ion Beam JFIB 4610) to observe the crystal structure and morphology, respectively. ImageJ software was used to process the FE-SEM images to quantify the density of the nanosheet. Pictures at 5,000 x magnification were used; nine horizontal and vertical lines were drawn on them. Each time a top part (peak) of the nanosheet was intersected with the drawn line, an intersection point was marked on the image. The points were then counted; the greater the number of intersection points, the larger the density/coverage of the nanosheet film.

Results and Discussion

Figure 2 shows typical SEM images of tall-type of ZnO nanosheets electrodeposited for a long time (in this case, using 1 mA/cm^2 current for 1 h). The double-layer microstructure, which consists of a nanosheet (approximately 9.8 µm in height) grown on a dense underlayer (approximately 2.2 µm in height) obtained under galvanostatic mode, is shown in the inset in Figure 2a. The nanosheet forms a major part of the total structure, a unique feature in galvanostatic electrodeposition [2,10]. The crystal growth mechanism has been discussed in detail in our previous study [10]. In short, at the initial stage, nanosheet growth was driven by the formation of the $Zn_5(OH)_8(NO_3)_2{\bullet}2H_2O$ (or ZNH) [17] and the $Zn_5(CH_3COO)_2(OH)_8{\bullet}2H_2O$ (or ZAH) [15]. The ZNH then disappeared after prolonged deposition because it competed with hydroxide production (Eq. 1). After sufficient time, the ZnO underlayer was formed together with the further growth of the ZAH nanosheet, the partial condensation of the ZAH to form ZnO [18], and the formation of the more complex form of the ZAH, i.e. $Zn_x(CH_3COO)_y(OH)_z{\bullet}nH_2O$ (or ZAHH) [15,18]. The XRD of the as-deposited film (Figure 3a) shows the presence of ZAH, ZAHH, and ZnO. The response of ZnO here was mainly contributed by the dense underlayer where the (002) peak is the tallest [10]. Annealing at 400°C for 1 h was then performed to the as-deposited sample to transform the ZAH (and ZAHH) to ZnO (Eq. 6 and 7) [19]. After annealing, the ZAH and ZAHH were completely transformed to ZnO (XRD in Figure 3b), and a porous sheet was obtained (Figure 2b).

$$Zn_5(CH_3COO)_2(OH)_8{\bullet}2H_2O_{(s)} \rightarrow Zn_5(CH_3COO)_{2(s)} + ZnO_{(s)} + H_2O_{(g)} \quad (6)$$

$$Zn_5(CH_3COO)_{2(s)} + H_2O_{(g)} \rightarrow ZnO_{(s)} + CH_3COOH_{(g)} \quad (7)$$

Tall-type nanosheets as shown in Figure 2 are beneficial for certain applications, such as dye-sensitized solar cells or photocatalysts where a high surface area is desired. However, for other applications, such as perovskite solar cells, which require a relatively shorter nanosheet structure (in the order of 1 µm or shorter)

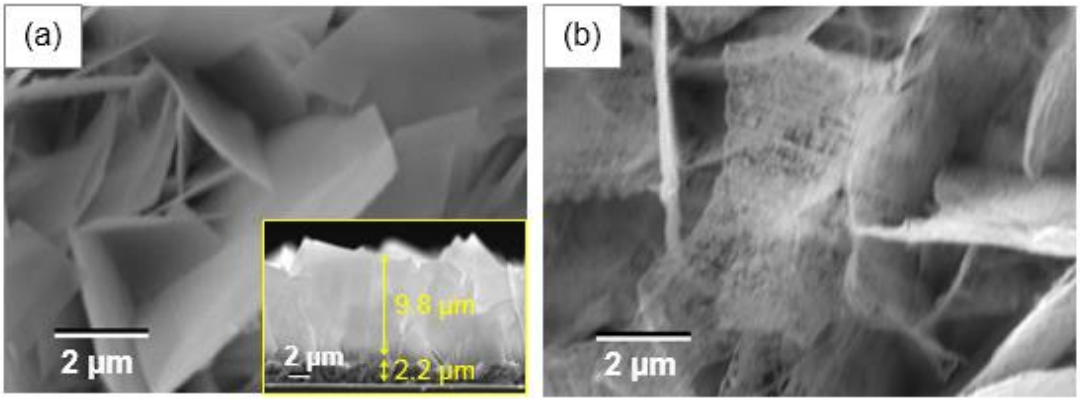

Figure 2. SEM Images of Typical Samples Electrodeposited at 1 mA/cm^2 for 1 h (a) Before and (b) After Annealing. The Inset Shows a Cross View of the Sample

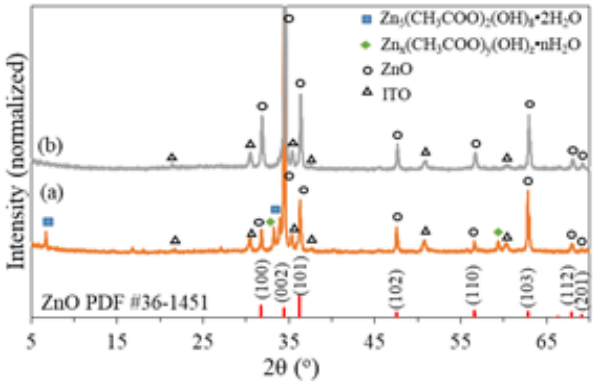

Figure 3. XRD of Samples Electrodeposited at 1 mA/cm^2 for 1 h (a) Before and (b) After Annealing. The Intensities are Normalized Against the ITO Peak at 2θ = 35.4°.

with good coverage, adjustments must be made. The first attempt to achieve such structure was performed by reducing the deposition time (only 60 s). While shorter nanosheets could be achieved (less than 1 µm as desired), the coverage density of the nanosheet was compromised (see Figure 4a). To improve the coverage, the first deposition parameter that was evaluated was the presence of oxygen in the electrolyte solution. The Ar gas previously bubbled in the solution was removed, thus allowing oxygen from the air to mix in the electrolyte solution. The result of the electrodeposited sample in the presence of oxygen is shown in Figure 4b. The nanosheet became denser and taller due to the extra hydroxide production route (Eq. 2). This result suggests that the hydroxide production route via oxygen reduction (Eq. 2) is easier than that via nitrate reduction (Eq. 1). Oxygen tends to cover larger areas of the ITO substrate compared with the nitrate ions; thus, more nucleation sites are formed, resulting in a denser nanosheet. However, the height of the nanosheet for the sample without Ar bubbling was approximately 2.6 µm, which is much taller than the desired height (~1 µm or less). Therefore, the effect of different components of the electrolyte solution must be further evaluated. Zabreska *et al.* [11] previously reported the formation of a nanosheet structure in electrodeposition using a deaerated solution of 0.1 M $Zn(CH_3COO)_2$ as the electrolyte (potentiostatic, at −1.2 V vs. Ag/AgCl at 25°C). Electrodeposition was then compared using the same solution containing oxygen and found that the oxygen present in the electrolyte disturbs the formation of the initially well-distributed sheet-like structure and produces an extra 3D structure on top of a nonuniform 2D nanosheet. Even though the specific microstructure changes due to the presence of oxygen is different with the current report (which may be due to the different electrodeposition mode or electrolyte composition), nevertheless, it support that the oxygen in the electrolyte can affect the microstructure that results from the electrodeposition method.

A previous study has reported that at early deposition time, nanosheet formation is driven by the formation of ZNH and ZAH, which are products of the presence of nitrate and acetate, respectively [10]. Therefore, varying both concentrations in the electrolyte used for electrodeposition can be an important factor in controlling crystal growth for deposition in a short time. The variations of the electrolyte composition and the respective codes of the samples produced from electrodeposition are presented in Table 1.

The first set of variation evaluated is the acetate concentration. $Zn(NO_3)_2$ concentration is kept at 0.05 M. The FE-SEM images are shown in Figure 5. When the concentration of the acetate is 0.01 M (A1N5), the electrodeposited sample observed is not a nanosheet but a particle-like layer. This result shows that an extremely low concentration of acetate leads to the failure to form a nanosheet structure. Moreover, it signifies the importance of acetate ions in forming the nanosheet structure because a sufficient concentration is needed to control crystal growth effectively during electrodeposition.

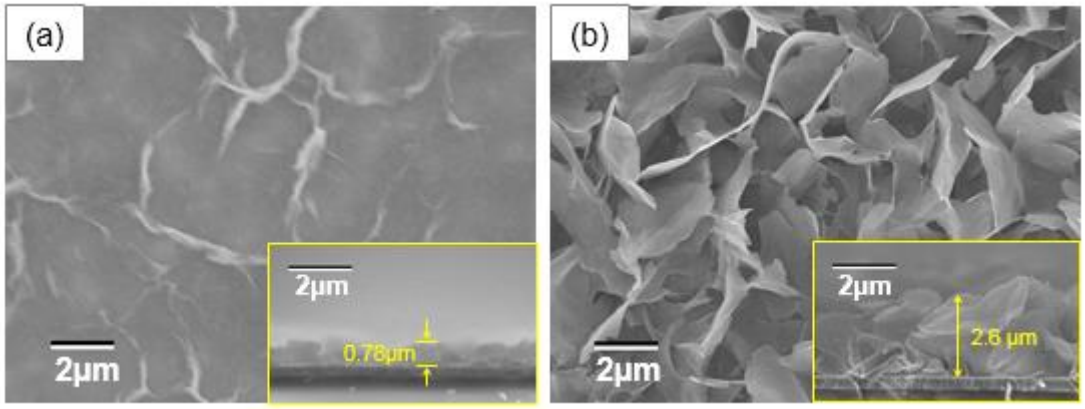

Figure 4. SEM and FE-SEM Images of the Electrodeposited Samples (a) bubbled and (b) Not Bubbled with Ar Gas, Respectively, During Electrodeposition. Deposition was Performed at 1 mA/cm^2 for 60 s, with an Electrolyte Containing 0.05 M CH_3COOK and 0.05 M $Zn(NO_3)_2$. Insets are the Respective Cross Views

Table 1. Sample Codes and their Respective Electrolyte Compositions

Sample code	Electrolyte composition
A1N5	0.01 M CH_3COOK + 0.05 M $Zn(NO_3)_2$
A3N5	0.03 M CH_3COOK + 0.05 M $Zn(NO_3)_2$
A5N5	0.05 M CH_3COOK + 0.05 M $Zn(NO_3)_2$
A7N5	0.07 M CH_3COOK + 0.05 M $Zn(NO_3)_2$
A5N3	0.05 M CH_3COOK + 0.03 M $Zn(NO_3)_2$
A5N7	0.05 M CH_3COOK + 0.07 M $Zn(NO_3)_2$

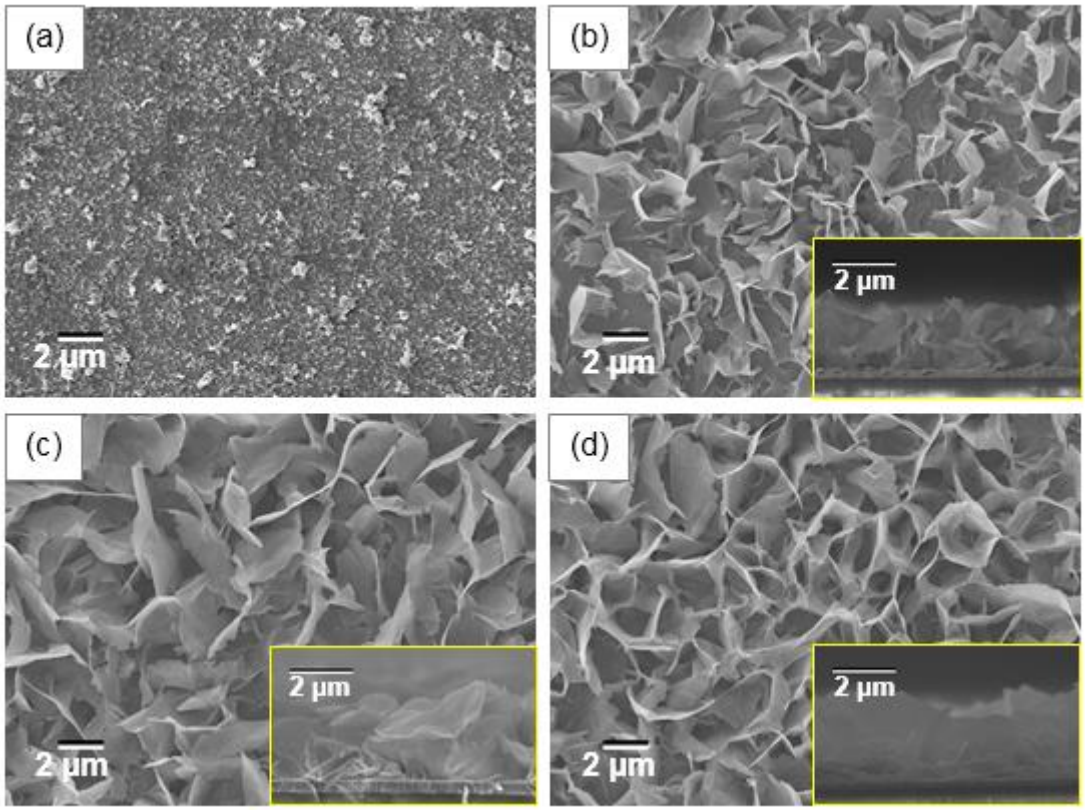

Figure 5. FE-SEM Images of the As-deposited Samples using Electrolytes with $Zn(NO_3)_2.4H_2O$ Concentrations at 0.05 M and Different Concentrations of CH_3COOK: (a) 0.01 M (A1N5), (b) 0.03 M (A3N5), (c) 0.05 M (A5N5), and (d) 0.07 M (A7N5). Insets are the Corresponding Cross Views

A similar result has been reported by Kung *et al.* [2] for potentiostatic electrodeposition using an extremely low concentration of acetate as the additive shaping agent (0 and 0.01 M). An extremely low concentration or the absence of acetate in the $Zn(NO_3)_2$-based electrolyte solution leads to the growth of ZnO with a non-nanosheet structure. Increasing the concentration of CH_3COOK to be 0.03 M (A3N5) is the minimum value observed in this study to form the desired nanosheet effectively. For samples electrodeposited using an acetate concentration of 0.03 (A3N5), 0.05 (A5N5), and 0.07 M (A7N5), nanosheets that look well distributed and cover the ITO substrate are observed. The three samples seem to have morphology profile differences. For instance, the A3N5 seems to have more nanosheets with a narrower gap compared with A5N5. In other words, A3N5 seems to be denser than A5N5. To provide a quantitative judgment, we performed image processing (using ImageJ software) to the top view of the FE-SEM images of all samples (three images for each sample) at the same magnification (at 5,000 x).

The example of the image processing for the A5N5 sample is shown in Figure 6d. Nine horizontal and vertical lines were drawn on each of the pictures; each time the tips of the nanosheet were intersected with the lines, it was marked and then counted. A denser/larger coverage of the nanosheet can thus be indicated by the large number of intersection points. The result of the average counted intersection points, as well as the error bar of one standard deviation of each sample, is presented as graphs in Figure 7. The height of the nanosheet of each sample (average from 10 lines in 1 image) is also measured and presented in Figure 7. The height of the three samples is not significantly increased, but the tendency to increase by increasing the acetate concentration can still be observed. On the other hand, the number of intersection points of A3N5 sample (low acetate concentration) is the largest compared to A5N5 and A7N5 samples. These results show that increasing the acetate concentration to more than 0.03 M results in the tendency to grow the height of the nanosheet rather than increasing the coverage. This result further suggests that low concentrations of acetate are more effective in producing denser and shorter nanosheets. In the evaluation of the XRD of these samples (Figure 7A), the crystal observed is only the zinc acetate hydrate one, without the presence of any ZnO peaks. This observation shows that the ZAH species were grown (Eq. 4) directly into nanosheet structures during electrodeposition at the period used in this study. Therefore, large amounts of acetate ions are expected to provide more chances for new nucleation sites to emerge, eventually growing into new nanosheets and producing a larger substrate area that is covered by the nanosheet (i.e. denser nanosheet film). However, the results show the opposite; low concentrations of acetate ions produce the densest films probably because by increasing the acetate concentration, more acetate ions were available at the vicinity of the ITO substrate, competing with the nitrate (and probably the oxygen as well) and reducing the possibility of an effective cathodic reaction (Eqs. 1 and 2). The expected formation of new nucleation sites is hindered at the substrate site where these acetate ions were located/adhered because of the absence of the hydroxide needed at that particular site.

The result of the nitrate variation also shows a similar trend. When the $Zn(NO_3)_2$ concentration is small (0.03 M, the A5N3 sample), the coverage is denser, and the height is shorter. However, changing the $Zn(NO_3)_2$ concentration to 0.01 M produces a particle-like layer similar to those observed for the A1N5 sample but with the initial formation of nanosheets in some parts (data not shown). This result suggests that a sufficient amount of nitrate ions is needed to grow nanosheet structures effectively. Similar to acetate variation, the A5N3, A5N5, and A5N7 samples seem to have morphology profile differences. A5N3 seems to be denser than A5N5. Thus, image processing was also performed. The result of the counting of the intersection points shows a significant increase in the number of intersection points for the low nitrate sample (A5N3) compared with the other two (A5N5 and A5N7). This finding shows that better coverage/higher density is obtained by the sample with a smaller amount of nitrate ions. This result is unexpected because high nitrate concentrations are supposed to produce more hydroxide where more nanosheets can be formed. Moreover, the high-enough concentration of nitrate can also be used as a shaping agent responsible for the growth of nanosheet crystals by producing ZNH (Eq. 5)[17].

Therefore, if a high-enough concentration is used, increasing the nitrate concentration should lead to a denser nanosheet. In the evaluation of the XRD of these samples (Figure 7B), only ZAH is observed, and no signs of ZnO or ZNH is present. This observation proves that the increase in the nitrate ion concentration we performed in this study was not high enough to make it responsible for the shaping of the nanosheet. Therefore, the increase in nitrate concentration in this study was only used to increase the production of the hydroxide (Eq. 1). However, it should still lead to an increase in the coverage density because more hydroxide should lead to more ZAH production and nucleation site formation. The decrease in the coverage density as the nitrate concentration was increased probably occurred because by increasing the number of nitrate ions nitrate competes with acetate in gathering around the conducting substrate. Although more hydroxide can be produced, only a few acetate ions were available to react at this particular site to form a new nucleation site. Eventually, a less dense nanosheet was formed. This result shows that controlling the

deposition rate by increasing nitrate concentration is not the most effective route because of its negative effects. Instead, carefully controlling the oxygen content in the solution is probably more appropriate to control the electrodeposition of ZnO nanosheet. This topic can be investigated in our future research. Meanwhile, the height of the nanosheet shows a slight increase when the $Zn(NO_3)_2$ concentration is increased (~2.2 µm for A5N3, ~2.64 µm for A5N5, and ~2.45 for A5N7). This result shows that increasing the nitrate concentration increases hydroxide production which is mainly used to grow the nanosheet's height instead of forming a new nucleation site. Moreover, it supports the discussion above and shows that the lower concentration of nitrate is more beneficial in producing denser and shorter nanosheets.

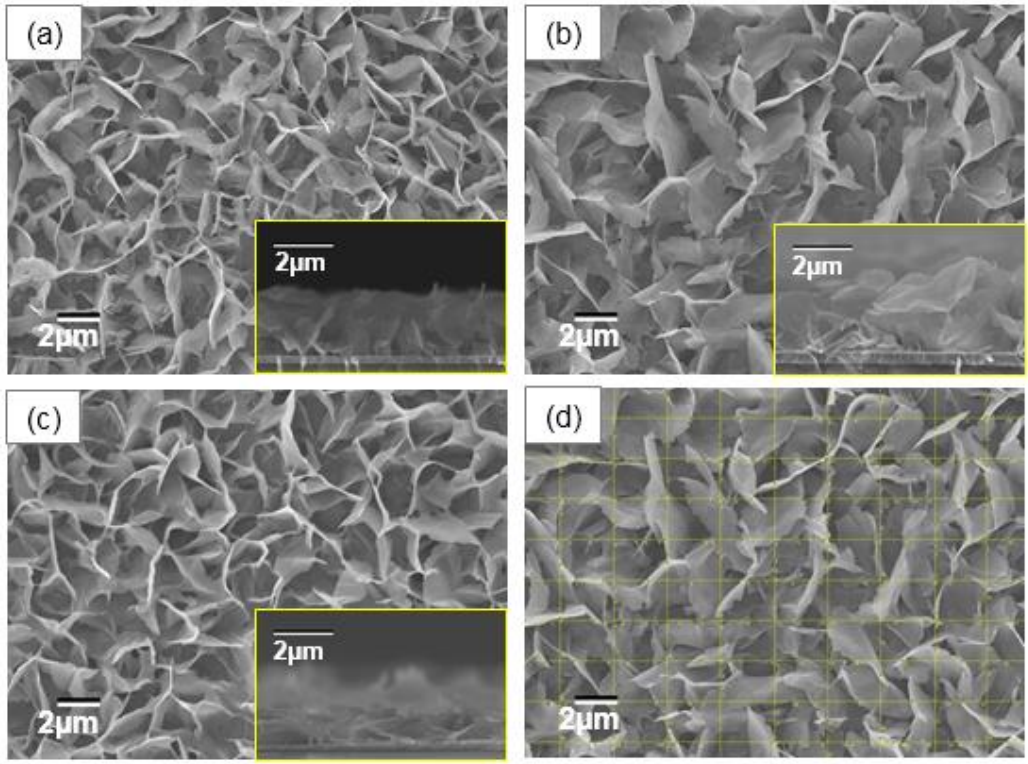

Figure 6. FE-SEM Images of the As-deposited Samples using Electrolytes with CH_3COOK Concentrations of 0.05 M and Different Concentrations of $Zn(NO_3)_2$: (a) 0.03 M (A5N3), (b) 0.05 M (A5N5), and (c) 0.07 M (A5N7). (d) Example of Image Processing using Image J Software Applied on Sample A5N5 to Quantify the Density of the Nanosheet Film

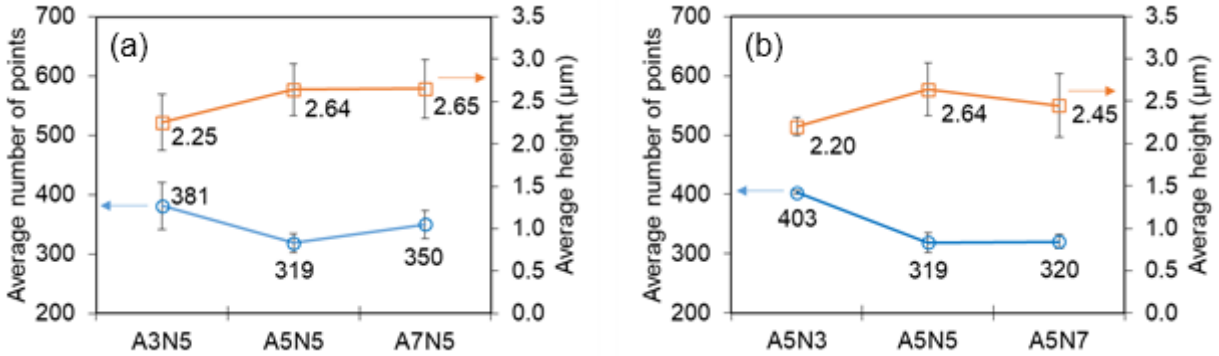

Figure 7. (Circle) Average Number of Intersection Points Between the Line Drawn on the FE-SEM Images and the Tip of the Nanosheets to Indicate the Coverage Density of the Nanosheet Layer. (Square) Height of the Respective Samples. (a) Samples with Various Acetate and (b) Nitrate Concentrations

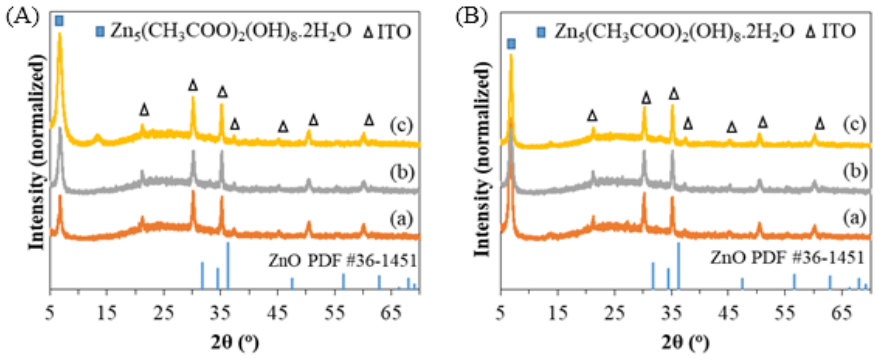

Figure 8. XRD of the As-deposited Samples (A) using Electrolytes with $Zn(NO_3)_2$ Concentrations of 0.05 M and Different Concentrations of CH_3COOK: (a) 0.03 (A3N5), (b) 0.05 (A5N5), and (c) 0.07 M (A7N5); (B) using Electrolytes with CH_3COOK Concentrations of 0.05 M and Different Concentrations of $Zn(NO_3)_2$: (a) 0.03 (A5N3), (b) 0.05 (A5N5), and (c) 0.07 M (A5N7). The Intensities are Normalized Against the ITO peak at 2θ = 35.4°

The results obtained above suggest that low amounts of acetate and nitrate concentration can provide beneficial effects in producing short and dense nanosheet morphologies. The combination of low concentration conditions in one solution (0.03 M CH_3COOK + 0.03 M $Zn(NO_3)_2$) and varying the amount of oxygen gas contained in the electrolyte solution can be further investigated. The morphology during electrodeposition for an even shorter time (ex. 30 s or lower) can also be evaluated to produce nanosheets with a height of less than 1 µm and with various coverage densities. These topics will be the subject of our future study. These optimizations are needed in terms of improving the morphology to meet the required characteristics for the ETL of perovskite solar cells. However, after annealing, a porous structure, which is not necessarily important for this specific application, is obtained. In our previous study, we observed that porosity is reduced when the annealing process was performed in an inert Ar atmosphere. A complete mechanism for this phenomenon might need further study and confirmation; however, it might be related to the possibility of the formation of evaporated gases (Eqs. 5 and 6) being hindered in the inert atmosphere. A comparison of porous and less porous ZnO nanosheets as ETL will also be an interesting topic for further study. Recently, researchers have been discussing about improving the stability of perovskite solar cells by performing interface engineering at a certain part of the cells (i.e. parts that directly interact with perovskite materials); a method aiming for such improvement includes the oxide surface modification of ETLs [20,21] or the carbon cathode in the hole-transport layer free type [22] and even the grain boundary of the perovskite materials itself [23]. On this basis, the $Zn_5(CH_3COO)_2(OH)_8•2H_2O$ nanosheet observed in this study before annealing can be considered an oxide modification of ZnO, which may be beneficial as an ETL. A comparison of the performance of the nonporous $Zn_5(CH_3COO)_2(OH)_8•2H_2O$ nanosheet and the porous (or less porous) ZnO nanosheet is also an interesting topic for future research.

Conclusion

The key parameters for the growth control of short-type ZnO nanosheets are evaluated. The presence of oxygen in the electrolyte solution significantly influences the morphology of the obtained nanosheet. The nanosheet becomes much denser and taller in the presence of oxygen. Meanwhile, the effect of varied electrolyte compositions is not as significant. Nevertheless, the trend of such effect can still be observed. Improved results are obtained when the concentration of each anion is low. However, extremely low concentrations lead to the formation of non-nanosheet layers. Therefore, the electrolyte concentration must be optimized. In this study, relatively denser and shorter nanosheets are obtained when the concentration of the acetate or $Zn(NO_3)_2$ is 0.03 M.

Acknowledgements

We acknowledge the research facilities provided by P2F-LIPI that were used in this study, including characterization devices such as XRD and FE-SEM. We state the authors' contribution as follows: GET for ZnO electrodeposition and characterization, paper drafting and discussion; DH for ZnO electrodeposition and discussion; WBW for paper discussion.

References

[1] Lin, C-Y.,Lai, T-H.,Chen, H-W.,Chen, J-G.,Kung, C-W.,Vittal, R., Ho, K-C. 2011. Highly efficient dye-sensitized solar cell with a ZnO nanosheet-based photoanode. Energy Env. Sci. 4: 3448–3455, https://doi.org/10.1039/c0ee00587h.

[2] Kung, C.,Chen, H.,Lin, C.,Lai, Y.,Vittal, R., Ho, K. 2014. Electrochemical synthesis of a double-layer film of ZnO nanosheets/nanoparticles and its application for dye-sensitized solar cells. Prog. Photovolt Res. Appl. 22: 440–451, https://doi.org/10.1002/pip.

[3] Zhang, J., Meguid, S A. 2017. Piezoelectricity of 2D nanomaterials: characterization, properties, and applications. Semicond. Sci. Technol. 32: 043006, https://doi.org/10.1088/1361-6641/aa5cfb.
[4] Zhang, R.,Hummelgård, M.,Olsen, M., Jonas, Ö. 2017. Nanogenerator made of ZnO nanosheet networks. Semicond. Sci. Technol. 32: 054002, https://doi.org/10.1088/1361-6641/aa660c.
[5] Ibn-mohammed, T., Koh, S.C.L., Reaney, I.M., Acquaye, A.,Schileo, G.,Mustapha, K B. and Greenough, R. 2017. Perovskite solar cells: An integrated hybrid lifecycle assessment and review in comparison with other photovoltaic technologies. Renew. Sustain. Energy Rev. 80: 1321–1344, https://doi.org/10.1016/j.rser.2017.05.095.
[6] Juarez-Perez, E.J., Wussler, M., Fabregat-Santiago, F., Lakus-Wollny, K., Mankel, E., Mayer, T., Jaegermann, W., Mora-Sero, I. 2014. the role of the selective contacts in the performance of lead halide perovskite solar cells. J. Phys. Chem. Lett. 5: 680–685, https://doi.org/10.1021/jz500059v.
[7] Stranks, S.D., Eperon, G.E., Grancini, G., Menelaou, C., Alcocer, M.J.P., Leijtens, T., Herz, L.M., Petrozza, A., Snaith, H.J. 2013. Electron-hole diffusion lengths exceeding 1 micrometer in an organometal trihalide perovskite absorber. Sci. 342: 341–344, https://doi.org/10.1126/science.1243982.
[8] Guo, W., Liu, T., Gou, Z., Zheng, W., Chen, Y., Wang, Z. 2013. Hydrothermal synthesis of ultrathin ZnO nanosheets and their gas-sensing properties. J Mater. Sci. Mater. Electron. 24: 1764–1769, https://doi.org/10.1007/s10854-012-1009-x.
[9] Cao, B., Cai, W., Li, Y., Sun, F., Zhang, L. 2005. Ultraviolet-light-emitting ZnO nanosheets prepared by a chemical bath deposition. Nanotechnol. 16: 1734-1738, https://doi.org/10.1088/0957-4484/16/9/054.
[10] Timuda, G.E., Waki, K. 2020. Galvanostatic electrodeposition of ZnO nanosheet: Effect of different applied current densities and deposition times on the nanosheet morphology. Adv. Nat. Sci. Nanosci. Nanotechnol. 11: 025005, https://doi.org/10.1088/2043-6254/ab7c60.
[11] Zarebska, K., Kwiatkowski, M., Gniadek, M., Skompska, M. 2013. Electrodeposition of Zn(OH)2, ZnO thin films and nanosheet-like Zn seed layers and influence of their morphology on the growth of ZnO nanorods. Electrochim. Acta. 98: 255–262, https://doi.org/10.1016/j.electacta.2013.03.051.
[12] Xu, F., Lu, Y., Xie, Y., Liu, Y. 2009. Controllable morphology evolution of electrodeposited ZnO nano/micro-scale structures in aqueous solution. Mater. Des. 30: 1704–1711, https://doi.org/10.1016/j.matdes.2008.07.024.
[13] Chen, H., Zhu, L., Liu, H., Li, W. 2013. Effects of preparing conditions on the nanostructures electrodeposited from the Zn(NO3)2 electrolyte containing KCl. Thin Solid Films 534: 205–213, https://doi.org/10.1016/j.tsf.2013.02.060.
[14] Liang, W., Li, W., Chen, H., Liu, H., Zhu, L. 2015. Exploiting electrodeposited flower-like Zn4(OH) 6SO4.4H2O nanosheets as precursor for porous ZnO nanosheets. Electrochim. Acta. 156: 171–178, https://doi.org/10.1016/j.electacta.2015.01.022.
[15] Hou, Q., Zhu, L., Chen, H., Liu, H., Li, W. 2013. Highly regular and ultra-thin porous ZnO nanosheets : An indirect electrodeposition method using acetate-containing precursor and their application in quantum dots-sensitized solar cells. Electrochim. Acta. 94: 72–79, https://doi.org/10.1016/j.electacta.2013.01.122.
[16] Hou, Q., Zhu, L., Chen, H., Liu, H., Li, W. 2012. Growth of porous ZnO nanosheets by electrodeposition with the addition of KBr in nitrate electrolyte. Mater. Lett. 89: 283–286, https://doi.org/10.1016/j.matlet.2012.08.137.
[17] Hou, Q., Zhu, L., Chen, H., Liu, H., Li, W. 2012. Growth of flower-like porous ZnO nanosheets by electrodeposition with Zn5(OH)8(NO3)2•2H2O as precursor. Electrochim. Acta. 78: 55–64, https://doi.org/10.1016/j.electacta.2012.05.113.
[18] Hosono, E., Tokunaga, T., Ueno, S., Oaki, Y., Imai, H., Zhou, H., Fujihara, S. 2012. Crystal-growth process of single-crystal-like mesoporous ZnO through a competitive reaction in solution. Cryst. Growth Des. 12: 2923–2931, https://doi.org/10.1021/cg300116h.
[19] Moezzi, A., Mcdonagh, A., Dowd, A., Cortie, M. 2013. Zinc hydroxyacetate and its transformation to nanocrystalline zinc oxide. Inorg. Chem. 52: 95–102, https://doi.org/10.1021/ic302328e.
[20] Lira-Cantú, M. 2017. Perovskite solar cells: Stability lies at interfaces. Nat. Energy 2: 17115, https://doi.org/10.1038/nenergy.2017.115.
[21] Mingorance, A., Xie, H., Kim, H., Wang, Z., Balsells, M., Morales-melgares, A., Domingo, N., Kazuteru, N., Tress, W., Fraxedas, J., Vlachopoulos, N., Hagfeldt, A., Lira-Cantu, M. 2018. Interfacial engineering of metal oxides for highly stable halide perovskite solar cells. Adv. Mater. Interfaces. 5: 1800367, https://doi.org/10.1002/ad mi.201800367.
[22] Chen, J., Chen, T., Xu, T., Chang, J-Y., Waki, K. 2019. MAPbI3 self-recrystallization induced performance improvement for oxygen-containing functional groups decorated carbon nanotube-based perovskite solar cells. Sol. RRL 3: 1900302, https://doi.org/10.1002/solr.201900302.
[23] Li, X., Chen, C., Cai, M., Hua, X., Xie, F., Liu, X., Hua, J. 2018. Efficient passivation of hybrid perovskite solar cells using organic dyes with -COOH functional group. Adv. Energy Mater. 8: 1800715, https://doi.org/10.1002/aenm.201800715.